# Monitoring of the fracture mechanisms induced by pull-out and compression in concrete

CrossMark

A.C. Mpalaskas [a], I. Vasilakos [b], T.E. Matikas [a], H.K. Chai [c], D.G. Aggelis [b],*

[a] Department of Materials Science and Engineering, University of Ioannina, 45110 Ioannina, Greece
[b] Department of Mechanics of Materials and Constructions, Vrije Universiteit Brussel, Pleinlaan 2, 1050 Brussels, Belgium
[c] Department of Civil Engineering, University of Malaya, 50603 Kuala Lumpur, Malaysia

## ARTICLE INFO

## ABSTRACT

In-situ characterization of strength is of paramount importance for concrete engineers. To get an estimation of the compressive strength, slightly destructive tests are conducted on the surface of the material. One is the LOK test (pull-out) which offers a reliable estimation of compressive strength. The developed stress field is quite complicated and researchers have argued about the nature of the fracture mechanism. In the present paper, acoustic emission (AE) is applied during both compression and pull-out experiments on concrete cubes. Results show that the two damage modes emit different AE signatures, with compression leading to higher frequencies and pull-out to longer signal durations, while the finite element method (FEM) is used to analyze the stress field. Identification of the active damage mode in real time, is beneficial in order to assess the condition of integrity of concrete in structures by nondestructive monitoring.

© 2014 Elsevier Ltd. All rights reserved.

## 1. Introduction

The issue of structural integrity assessment is of primary concern nowadays, due to the aging of existing infrastructure. Effective monitoring and maintenance schemes are sought for in order to characterize the damage status and select the proper repair methodology. One of the factors that can provide valuable information about the structural condition is the dominant fracture mode. This is because in engineering structures the failure procedure follows a succession of modes starting from (micro-) cracking of the matrix material and leading eventually to catastrophic shear phenomena like delaminations, detachment of reinforcing bars or fiber pull-out. The dominant mode can possibly be characterized after fracture tests when the cracked surface is investigated with Scanning Electron Microscopy (SEM) [1,2]. However, it would be of great importance to characterize the fracture mode in real time. On this respect the acoustic emission (AE) technique has shown the potential to provide crucial information on the damage mode in a non-invasive and real time fashion. This has been demonstrated in many fields, ranging from metals [2–4], composites [5,6], rock [7], as well as cementitious materials [8,9]. The present work is concerned with the comparison of AE signatures during two different widely used fracture tests of concrete that lead to different failure modes, specifically the compression test and the "LOK" test.

The compression test is generally applied on cubes or cylindrical specimens. The maximum load over the cross section area is termed as "compressive strength" due to the nominally compression stress field that is developed and is the most significant engineering property of concrete [10]. However, the actual field may be more complex, influenced by the friction

---

* Corresponding author. Tel.: +32 2 629 3541; fax: +32 2 6292928.
  E-mail address: daggelis@vub.ac.be (D.G. Aggelis).

between the rigid metal plates and the concrete specimen that tends to expand laterally. In order to be able to evaluate as close as possible the compressive strength in-situ, different slightly destructive test have been developed. These tests cause minor damage on the surface of concrete and therefore, they do not compromise structural performance. One of the most widely applied tests is the pull-out test, the first reference on which can be found in 1938 [11]. It involves a metallic insert which is cast into fresh concrete with the aim of pulling it out when the material hardens. This is mainly for checking the compliance with concrete strength regulations, while drilled-hole methods are also applicable for estimations on an existing structure. The advantage of such a test is that it immediately supplies a result on the "strength" of the material on the spot, without the need to extract cores saving time and resources, while the surface disruption caused is certainly smaller than sampling a cylindrical core. When the insert is extracted, a cone of concrete is also pulled out of the specimen or structure, meaning that the result depends on strength properties of the material, making the test a reliable assessment of strength [12,13]. However, the exact failure mechanism is not clear, while different researchers have worked on the subject with sometimes contrasting studies as to the strength property that dominates failure [14,15]. What should be generally accepted is that LOK results in a non-uniform three dimensional field with strong shearing components, which certainly differs from the stress field of the standard compressive test.

In this study the compression and pull-out test (in the form of LOK) are used to study the acoustic emission signature of different damage modes while the results are escorted by a finite element analysis on the developed stress field. To the authors' knowledge it is the first time AE monitoring during the LOK test is presented. Preliminary results on pullout of reinforcing bars out of concrete have been published [16] after the pioneering work of Ohtsu et al. in a different pull-out setup of hook anchors [17]. Concerning compression on sampled cores, the AE activity has been used to evaluate the status of the bulk material and damage development [18,19]. Among others, the AE behavior is related to compressive strength, cracking development during bending as well as fracture energy [18–20] while recently AE events have been correlated to the creep behavior of concrete [21]. This is a part of a series of ongoing studies concerned with the identification of the dominant fracture mode in concrete based on the parameters of the emitted AE signals [22,23]. Previously it has been shown that the stage of matrix micro-cracking has distinct AE signature than the fiber pull-out stage in steel fiber reinforced concrete (SFRC) in terms of frequency (e.g. average frequency, AF) as well as other waveform parameters like "RA value" [8,22]. Additionally bending and shearing of mortar beams resulted in distinct differences with shear fracture emitting lower frequencies and longer AE waveforms [23]. In the above mentioned works the differences between the AE characteristics show the potential to identify the dominant fracture mode at least in controlled laboratory conditions using simple schemes based on a few AE parameters. Characterization of the active damage mode in real time is of great importance for the field, in order to supply information and basically warning against final failure, while it bears significance for material science studies, since it can help to characterize the type of damage that the material is susceptible to and contribute to a better design. This is the first step in an effort to apply characterization in real structures after of course other parameters like the wave attenuation and distortion due to microstructure are accounted for [23,24].

## 2. Experimental

### 2.1. Materials

One concrete mixture was produced consisting of fourteen specimens. There were two types of cubical specimen size: one was $200 \times 200 \times 200$ mm and the other was $150 \times 150 \times 150$ mm. Two of the larger specimens were produced, one for conducting the LOK test and the other for compression. Twelve specimens of $150 \times 150 \times 150$ mm size were also produced for measuring the average compression strength per age: three days (three specimens), seven days (three specimens) and twenty-eight days (six specimens). The aggregates consisted of 56% crushed sand, 13.87% fine gravel and 30.13% coarse gravel with maximum aggregate size 31.5 mm, while the water/cement ratio was 0.70 by mass. The density and the water absorption of the crushed sand were 2601 kg/m$^3$ and 0.98%, of fine gravel 2621 kg/m$^3$ and 0.75%, and of coarse gravel 2681 kg/m$^3$ and 0.61% respectively. The exact mix proportions were as follows: cement (type II 42.5 N) 80 kg/m$^3$, cement (type II 32.5 N) 200 kg/m$^3$, water 195 kg/m$^3$, crushed sand 1050 kg/m$^3$, fine gravel 260 kg/m$^3$, coarse gravel 565 kg/m$^3$, retarder – plasticizer (CHEM I) 1.54 kg/m$^3$, retarder – plasticizer (CHEM II) 1.96 kg/m$^3$. The actual bulk density of concrete was 2359 kg/m$^3$ while the ambient temperature at mixing was 25 °C. The workability as measured by the slump test was 11 cm. The specimens were cured in water saturated with calcium hydroxide at 23 ± 2 °C. The average compressive strength

of three days was $f_c(3)$ = 18.0 MPa, of seven days $f_c(7)$ = 24.7 MPa and of twenty-eight days was $f_c(28)$ = 33.8 MPa with a standard deviation of 3.0 MPa.

## 2.2. Compression and LOK test

Compression and LOK tests were conducted at the age of 28 days. Concerning compression, the load was applied on the 200 × 200 × 200 mm specimen at a constant rate of 0.3375 MPa/s until fracture and the test was automatically terminated at the moment of load drop. The compressive strength was 30.8 MPa.

The LOK test is generally applied to provide a reliable measurement of the actual strength of concrete mainly in newly cast structures in accordance with the pullout test method described in ASTM C900, or EN 12504-3 [25,26]. The steel disc (diameter of 25 mm) is cast at a depth of 25 mm into concrete either by attaching it to the formwork before placing concrete or by inserting it manually into fresh concrete, see Fig. 1a. Fig. 1b shows the fresh specimen after placing the insert which is attached to the red buoyancy cup. In practice the axis of the insert is slightly inclined relatively to the surface. Fig. 1c shows the insert and buoyancy cup system in more detail. After hardening, the steel disc is pulled against a 55 mm diameter pressure ring bearing on the surface similarly to Fig. 1a and the required force to pull the insert out is measured. The material in the strut between the disc and the counter pressure ring is subjected to a complex stress pattern. The pullout force is strongly correlated to the compressive strength [27].

Unlike the compression test, the loading rate for the LOK test cannot be constant because it is handled by a hydraulic jack driven by human hand thus, the loading rate is approximately 0.5 ± 0.2 kN/s [25]. As the insert is being pulled out, a conical fragment of the material is extracted. The compressive strength can be evaluated from established calibration curves [27]. The pull out load measured during the specific LOK test was 25.1 kN corresponding to a compressive strength of 31.9 MPa. More details about the geometry and the whole procedure of LOK test can be found in literature [12,13,27].

## 2.3. AE monitoring

AE was monitored by two types of piezoelectric sensors, namely the R15 (Physical Acoustics Corp., PAC) with resonance nominally at 150 kHz, and the Pico (PAC) which are considered more broadband with a sensitivity peak around 450 kHz. In total six sensors were applied, specifically four Pico and two R15. The signals were pre-amplified by 40 dB and were digitized by a sampling rate of 3 MHz in a PCI-8 board of PAC. In both cases of compression and LOK tests the four Pico were attached near the top surface of the cube and the two R15 in opposite corners near the bottom, see Fig. 2. All signals with amplitude higher than 40 dB (0.01 V) were recorded, while for the analysis, the signals with energy "zero" were disregarded. For location purposes the pulse velocity was measured by pencil lead breaks to the value of 4500 m/s.

Fig. 3 shows a typical AE waveform. Among many parameters that have been analyzed in AE literature, this illustration focuses on the RA value, which is the ratio of Rise Time (μs) over Amplitude (V) [8,22,28,29]. Additionally, peak frequency (PF) is the frequency with the maximum magnitude after fast Fourier transform of the time domain signal. These are the parameters that will be discussed in the results, while other indicators of frequency, like average or central frequency show similar trends.

# 3. Results

## 3.1. AE hits

The gravity in this study is given on some of the qualitative parameters of AE but introductory the cumulative population of individual signal (hits) will be discussed. Since two types of sensors with different characteristics were used, it is deemed
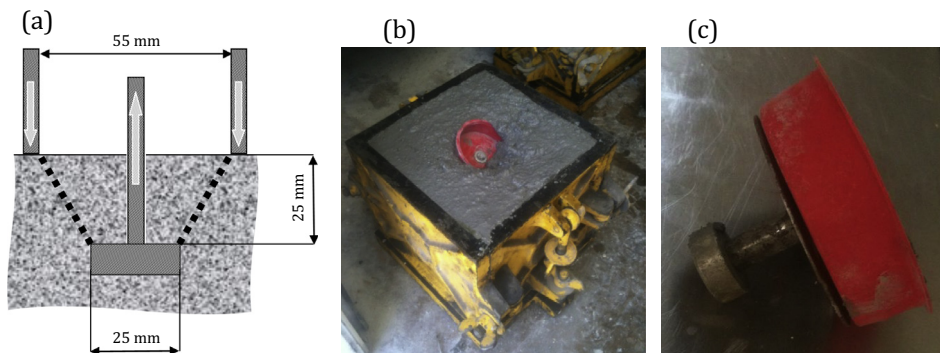


**Fig. 1.** (a) Schematic cross section of cast-in-place LOK-TEST insert, (b) LOK-TEST insert placed in fresh concrete, (c) close up of the insert and the floating cup.
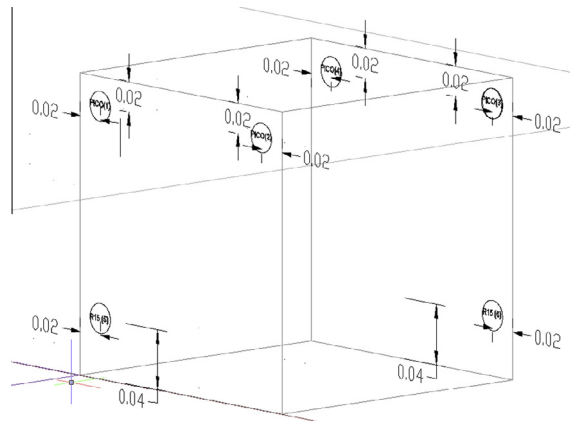
**Fig. 2.** Representation of the AE sensors location on the cube (distances in m).
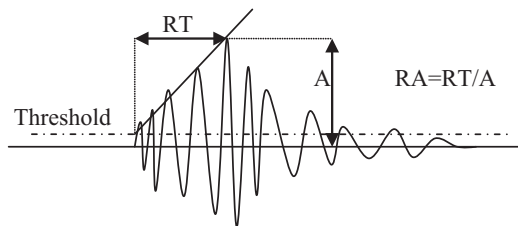


**Fig. 3.** Typical AE waveform.

essential to present the results separately for each type. Comparison of their behaviors is essential since the broadband type are better-suited for more detailed but laboratory-scale studies, while the resonant ones are fit for in-situ application. Fig. 4a shows the cumulative activity for the LOK test. Initially the activity is gradually building up until about 50 s, when a sharper increase is noted. This is the moment of maximum pull-out load. Consequently the rate of the recorded activity decreases exhibiting an asymptotic behavior. The resonant sensors reasonably acquire much higher number of emissions, even though they are two compared to four broadband sensors. Concerning the rate of the emissions, although the moment of peak load can be determined (as mentioned around 50 s) further comments cannot be done due to the fact that the rate of loading is not constant, as it is hand driven by a hydraulic jack. Fig. 4b shows the corresponding activity for the compression test. The trends are quite different with a quick increase (at 100 s) followed by a nearly constant (but not negligible) rate for approximately a minute. Afterwards, the activity for both sensor types increases as the final fracture stage of the specimen has started. Again resonant sensors exhibit more than double activity compared to the broadband ones.

Concerning qualitative features which are the focus of this study, Fig. 5a shows the peak frequency (PF) of the hits as measured by the broadband sensors for both loading configurations. Starting from the hits generated during the LOK test (Fig. 5a) it can be seen that the population can be divided in three major parts; one below 100 kHz, one between 100 kHz and 200 kHz and another smaller part with PF higher than 200 kHz. Specifically, the majority (75%) of the hits exhibit PF lower than 100 kHz, 20% is between 100 kHz and 200 kHz and only 5% scatters in the highest band above 200 kHz.
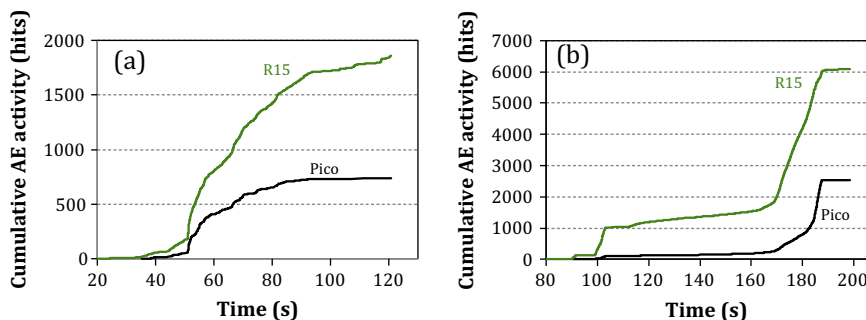


**Fig. 4.** Cumulative activity for (a) the LOK test and (b) the compression test as recorded by the different sensor types.

For the compression test, the same general classification holds with the difference that the third part of the population with frequency higher than 200 kHz is more densely populated than the LOK test, while the other bands are apparently weakened. Specifically from the total number of hits received by the Pico sensors during the compressive failure process up to 160 s, 30% have peak frequency below 100 kHz, 42% between 100 and 200 kHz and 28% PF higher than 200 kHz, which indicates a considerable shift to high frequencies compared to the LOK test. The sliding average lines which are also included in Fig. 5a show that for the period of stable micro-cracking (up to 160 s for the compression test) the "compressive" signals constantly exhibit higher frequency as an average than the LOK since the line fluctuates around 200 kHz, while for the LOK it is around 100 kHz.

It is mentioned that concerning the compression test, the above analysis of qualitative features are based on the AE population recorded up to 160 s when a stable cracking was being recorded. After that, the final stage of fracturing started during which, the cube was severely cracked while parts of the surface layer were detached (see Fig. 6). Due to the obvious disruption of the continuity of the medium, no correlation of the received waveform with the actual emitted signal can be supported for that stage and this is why the signals of the final part of the compression loading (after 160 s) are not taken into account for parameter analysis rather than only the cumulative activity graphs presented earlier.

For the same experiment the two resonant sensors showed two main bands (see Fig. 5b), below and above 100 kHz. Due to the resonance of the sensors, signals of higher frequencies were not recorded. The LOK test exhibited 75% of the population under 100 kHz and 25% above, while for the compression the majority of the hits is above 100 kHz, specifically 56% and the rest 44% below. The differences between the moving average lines as seen in Fig. 5b are still clear despite the resonant behavior of the sensors, i.e. the LOK line fluctuates around 75 kHz while the compression line around 120 kHz.

Another parameter that has been used for classification of AE signals based on their fracture mode is the RA value. The RA history for both tests based on the Pico sensors is shown in Fig. 7. The moving average line shows clearly that before the last stage of large scale fracture, the compression signals' RA lies in values approximately half or less than the signals of LOK, something that is in correspondence with previous results concerning matrix cracking and fiber pull-out of SFRC [8,22]. Results of RA based on the signals of R15 are not discussed as they did not exhibit strong trends.

## 3.2. AE events

The number of sensors (totally six) mounted on the specimens allowed to map the AE sources in three-dimensional space. When different sensors acquire signals within a limited time window, these are classified in an acoustic emission "event", which is the source fracturing incident that results in the individual signals recorded by the different receivers. By the time delay between acquisition of the signals at the different positions and provided that the elastic wave velocity of the material is known, the location of the source cracking event can be calculated [30,31]. Results of this analysis are presented below with discussion of the limitations. Fig. 8a shows the location of AE sources for the LOK test. The sources are located at the upper half of the cube. Specifically almost the whole population rests above the height of $Z = 120$ mm, averaging at 150 mm which actually corresponds to the depth of the insert (50 mm below the top surface of the cube). The empty volume after the cone was extracted is seen in Fig. 8b having a depth of 50 mm which is the depth that the metal disc was inserted during casting of the concrete cube. It is admitted that the accuracy of the AE sources location cannot be absolute as it depends on the sensor size relatively to the propagation distances as well as the heterogeneity of the medium [30,31]. In the specific case the insert is fixed to the plastic buoyancy cup (see Fig. 1) which reaches the surface of the cube, creating –in terms of wave propagation– a large void near the top surface of 50 mm diameter. Therefore, when a cracking incident occurs, the straight path is not available for propagation to each one of the sensors. This condition worsens as the cracking system between the insert and the surface is formed increasing the volume of the material which cannot support un-deviated wave propagation. This renders results of location approximate; still under these conditions, the results of Fig. 8a appear satisfactory.
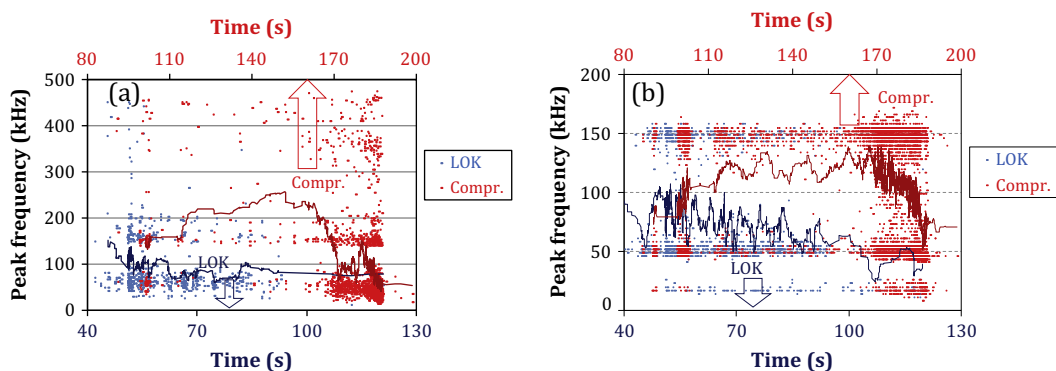


**Fig. 5.** Peak frequency history for different loading patterns as recorded by (a) the Pico sensors and (b) the R15 sensors. Lines are moving averages of 50 successive points.
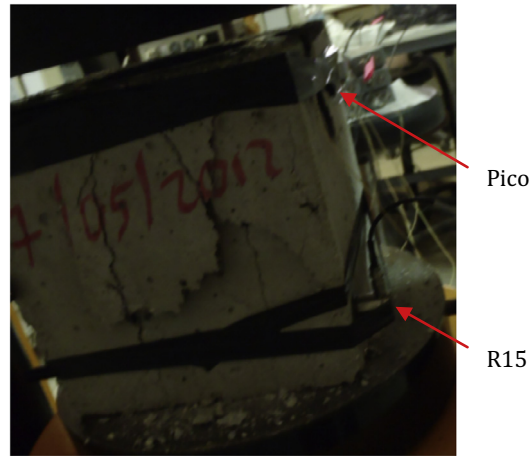
**Fig. 6.** Concrete cube after final failure under the compressive test.
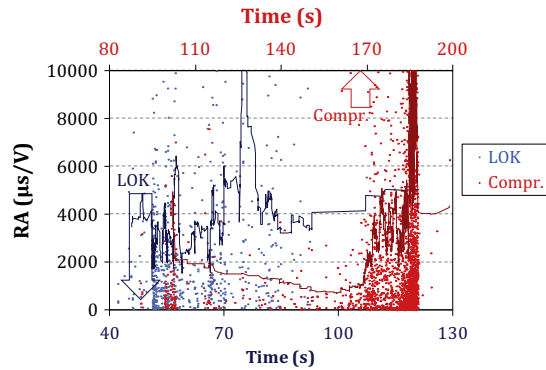


**Fig. 7.** RA-value history for different loading patterns as recorded by the Pico sensors. Lines are moving averages of 50 successive points.
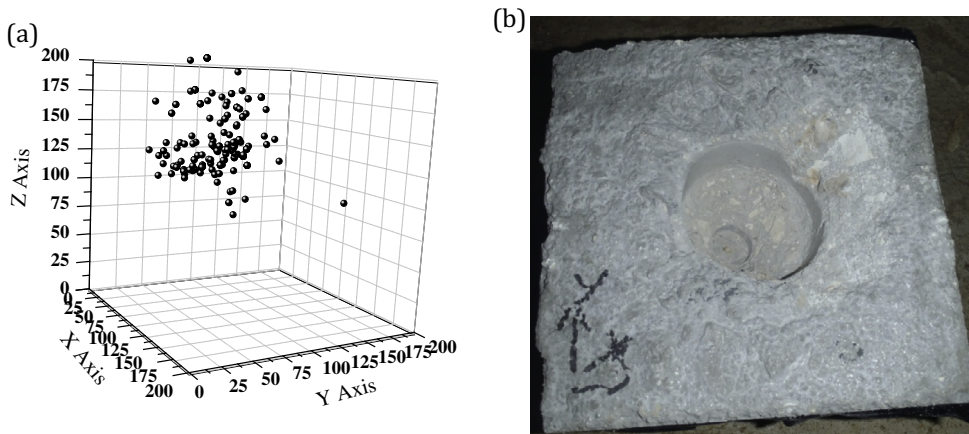


**Fig. 8.** (a) Location of AE sources for the LOK test and (b) photograph of the specimen after LOK test. The depth of the conical hole is 50 mm.

Fig. 9 shows the corresponding location results for the compression test. The sources in this case may be more dispersed in the volume of the cube, something reasonable due to the nominally uniform stress field but the results are not even as satisfactory. The reason is mainly that after the major cracking events, the whole volume of the medium loses its continuity and most of the emissions do not reach the required number of five sensors in order to be qualified as "events". This is why a
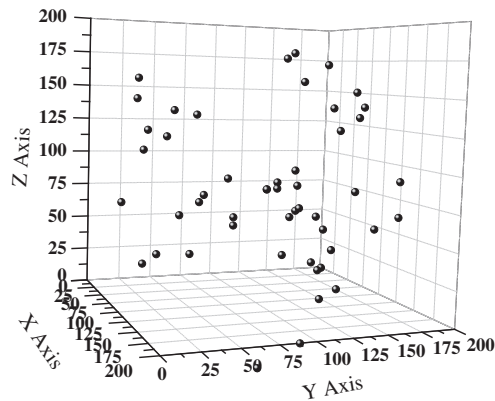
**Fig. 9.** Location of AE sources for the compression test.

relatively small number of events are shown on the graph of Fig. 9 corresponding to testing times before 170 s. After that moment the AE activity continued resulting to extensive number of individual AE hits as shown in Figs. 5 and 7. However, this activity, could not be received by the required number of sensors to be geometrically located so it does not appear in the events plot.

This can also be seen in Fig. 10 where the RA history based on the broadband (a) and the PF based on the resonant (b) are plotted based on the events. The trends shown in Fig. 10a are quite similar with the whole hit population discussed above and shown in Fig. 7. Additionally, the PF results from the resonant – based again on the events – show the same trends as the whole population of hits, with the average line of signals from compression being between 100 kHz and 150 kHz, while the LOK signals exhibit averages below 100 kHz. It is characteristic that from the dense population of hits at the last stage of the compression experiment (shown in Figs. 5 and 7) most of them are individual due to the severely cracked texture of the material at this stage and are not qualified as events. Therefore, the points of Fig. 10 are much less dense at the end.

## 4. Finite element model

The finite element method (FEM) is usually applied for stress analysis of static problems [32]. It was used to investigate the stress field involved in the LOK test, while a previous effort was published in the 1980s [15] aiming at predicting the cracking system for the same test. In the present case, FEM was used to determine the level and the area of influence of the shear as well as the normal stresses. For this purpose, a three dimensional model of the concrete specimen was generated according to the dimensions used in the experimental process (see Section 2.2). Tetrahedral solid elements of the Lagrangian formulation with four nodes, one integration point and linear displacement interpolation functions were used. The quality of the mesh was evaluated through a mesh convergence test based on the strain energy of concrete. The refinement of the mesh was based on the h-refinement process [33]. The mesh convergence analysis provided the result that an element size of 2 mm guarantees the necessary accuracy of the solution without significant increase of the computational time. To reinforce the stability of the numerical analysis an implicit integration scheme was selected. The concrete specimen was considered as linear elastic material with Young's modulus of 40 GPa and Poisson's ratio of 0.2, which is sufficient for the purpose of this study, i.e. to analyze the stress field developed due to the LOK insert pull out force. It is mentioned that the actual microstructure of concrete including aggregates, sand grains, air voids and porosity down to the size of μm could not be simulated due to the several millions of elements that would be required, number that renders the simulation unrealistic. In any case this is a static stress simulation while the microstructure would play important role in the simulation of the propagation of cracks, the path of which could be influenced by the interphase between the paste and aggregates. Dynamic fracture simulations have also been studied in different cases recently to reproduce the generation of AE events and predict the subsequent developments of cracks in concrete and other materials based on some assumptions concerning the elastic/plastic behavior of the material [34–36]. The steel disk, as well as the counter-pressure ring, were simulated as rigid bodies since they are much stiffer than concrete and their deformations are of no interest. For the execution of the numerical analysis the commercial finite element software ABAQUS/CAE 6.10 was used. Finally, all the calculations performed on an Intel Core i7 processor at 2.50 GHz.

Fig. 11 illustrates the mesh used for the concrete specimen (a) as well as the assembly and the loading conditions applied (b). A pull force with magnitude of 25 kN was applied on the LOK-TEST insert for calculation of the developed stress field. The angle of the force with respect to the vertical edges of the specimen was 20° as in the experiment. The counter-pressure ring with inner diameter of 55 mm was placed concentric with the disk on the surface of concrete. Concrete surfaces are free of constraints and therefore, the loading conditions are limited to the pulling force and the reaction of the counter-pressure ring. The results of the analysis are plotted relatively to the central cross section of the cube.
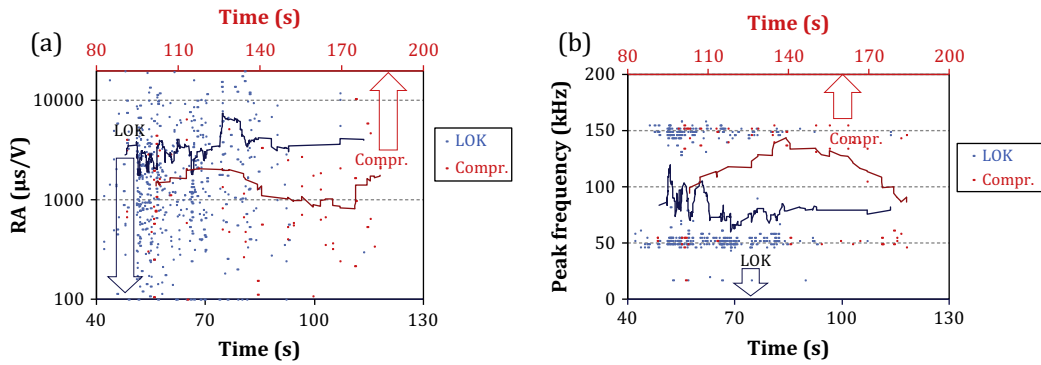
**Fig. 10.** (a) RA history for different loading patterns based on the qualified events, as recorded by the Pico sensors and (b) peak frequency for different loading patterns based on the qualified events, as recorded by the R15 sensors. Lines are moving averages of 30 successive points.
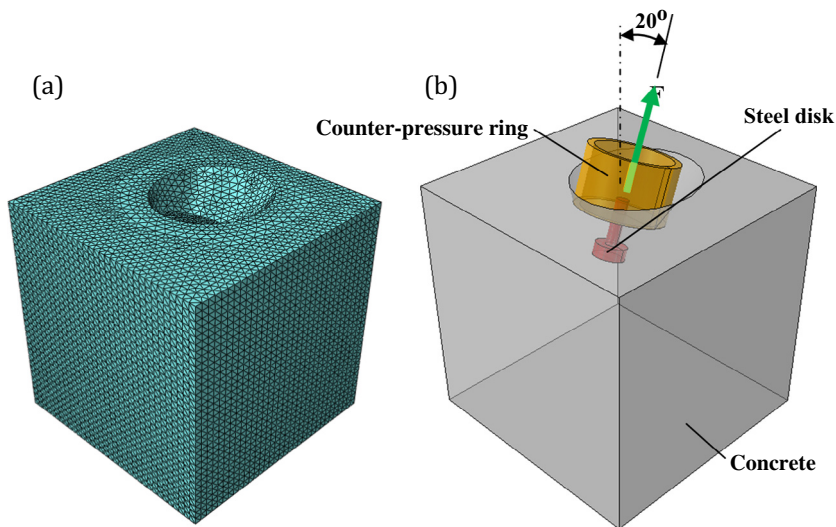


**Fig. 11.** Finite element mesh with elements of 2 mm (a) and assembly with loading conditions (b).

Fig. 12 shows the distribution of the normal stress $\sigma_{yy}$ (at the loading direction) in the plane of section A–A. To determine the areas under tension and compression, the stress component is decomposed into a tensile (Fig. 12a) and a compressive part (Fig. 12b). The maximum value belongs to compressive stress just below the reaction ring (see Fig. 12b). Perpendicular stresses ($\sigma_{xx}$, vertical to the loading direction) are of much lower value and their presentation is not deemed important.

Fig. 13a presents the distribution of the shear stress component $\sigma_{xy}$ in terms of absolute values. Considerable shear stresses are observed in paths AB and CD, as seen in Fig. 13b. Notice that these paths form a conical perimeter around the LOK insert that coincides with the final area of fracture observed during the experimental process.

To provide a more clear visualization of the stress mechanism that is developed during the test, the ratio of the in-plane shear component to the normal stress component is computed in terms of absolute values. Fig. 14a presents the areas where the value of the ratio $\sigma_{xy}/\sigma_{yy}$ is greater than 1.2. These are areas dominated by shear stresses. Fig. 14b shows the areas where the ratio is between 0.8 and 1.2. The characteristic of these areas is that the normal and the shear stresses are acting simultaneously with approximately the same order of magnitude. Finally, Fig. 14c shows the areas where the ratio is less than 0.8. In these areas shearing has a minor effect and the major stress mechanism are due to normal stresses. It can be seen that in contrast to the traditional compression test where fracture is (nominally) caused from purely compressive stresses, in the LOK test the effect of shearing to fracture is of extreme importance.

This is highlighted in Fig. 15 which provides a representation of the stress ratios in the area around the steel disk, where the absolute value of stresses is high, neglecting areas away from the insert where stresses are negligible. The thick dot lines represent the fracture path that has been experimentally observed. Purely normal stresses are limited on the concrete surfaces around the steel axis as well as on small areas around the upper surface of the steel disk insert. Areas along the fracture
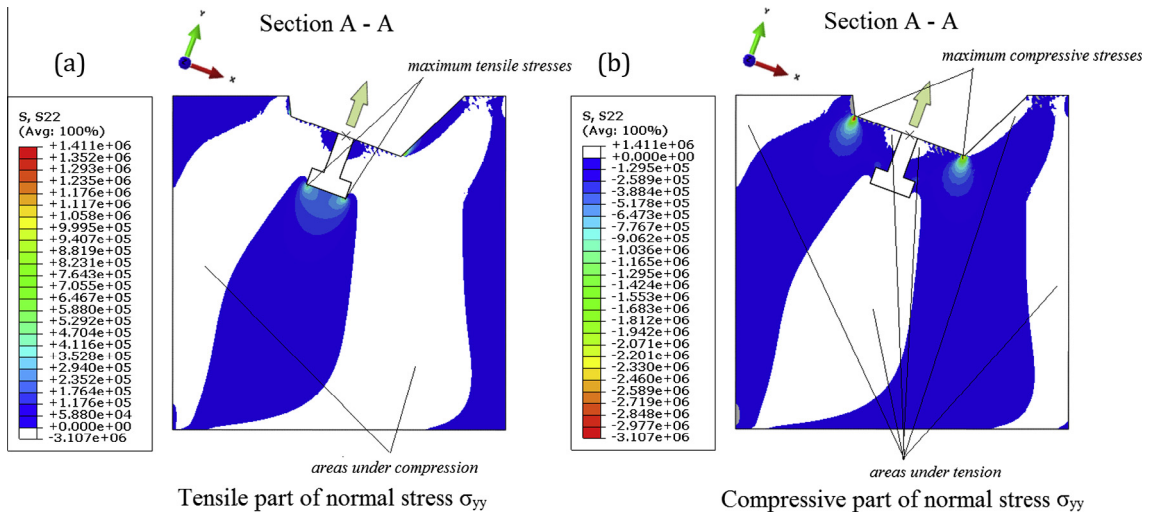
**Fig. 12.** Distribution of the normal stress component $\sigma_{yy}$. Decomposition into a tensile (a) and a compressive part (b).
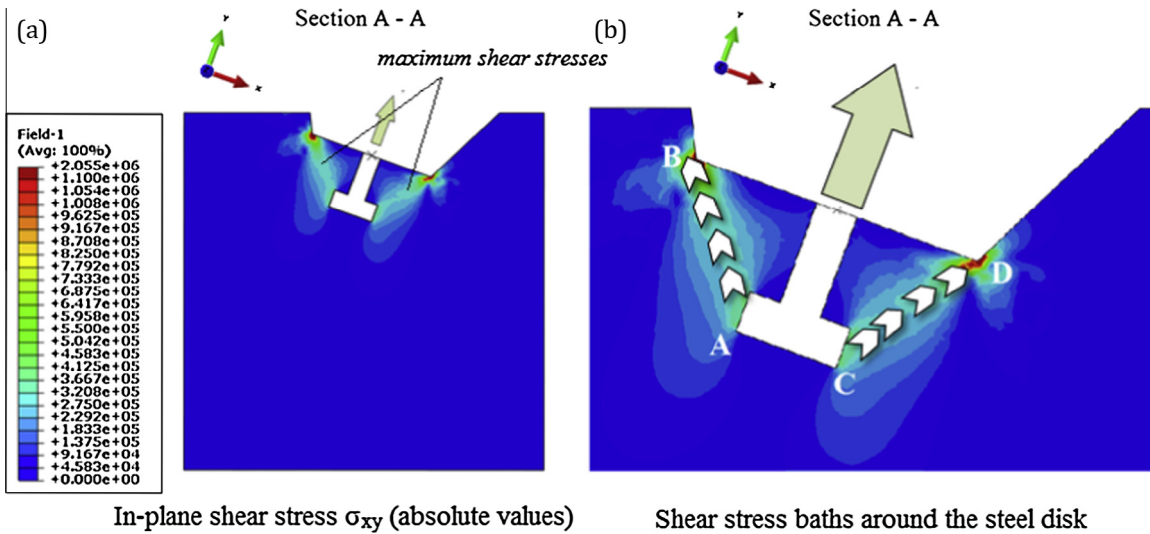


**Fig. 13.** (a) Distribution of the in-plane shear stress component $\sigma_{xy}$, (b) focus on the area of the insert.

paths are dominated by high shearing stresses ($\sigma_{xy}/\sigma_{yy} > 1.2$). Finally, transition areas characterized from shear and normal stresses of similar magnitude are observed between areas under pure normal stresses and areas under shearing.

## 5. Discussion

As the results of the FEM analysis demonstrate, the stress field initially developed during the LOK test combines both normal (tension and compression) and shear stresses. On the conical fracture surface, which is of great interest, strong shear stresses appear while their absolute values are higher than the normal stress at the same area. This mechanism substantially differs from the one involved in the concrete compression test where fracture is nominally caused by compressive stresses with absence of shearing. In an earlier study of AE during pull-out with different boundary conditions (absence of confinement ring) [17], the application of moment tensor analysis concluded that tensile stresses contributed strongly to fracture. However, in the present case, the existence of the confinement ring in the LOK test obviously increases the shear components as indicated by FEM and the AE parameters, leading to a more mixed mode of failure.

In this case, the FEM simulation model was not expanded to follow fracture rather than the initial elastic stress field. The reason is that it in the present stage it would be premature to conduct reliable prediction for the fracture of concrete with such complicated microstructure. Air bubbles, porosity, and fine sand grains would require an ultra fine mesh unrealistically
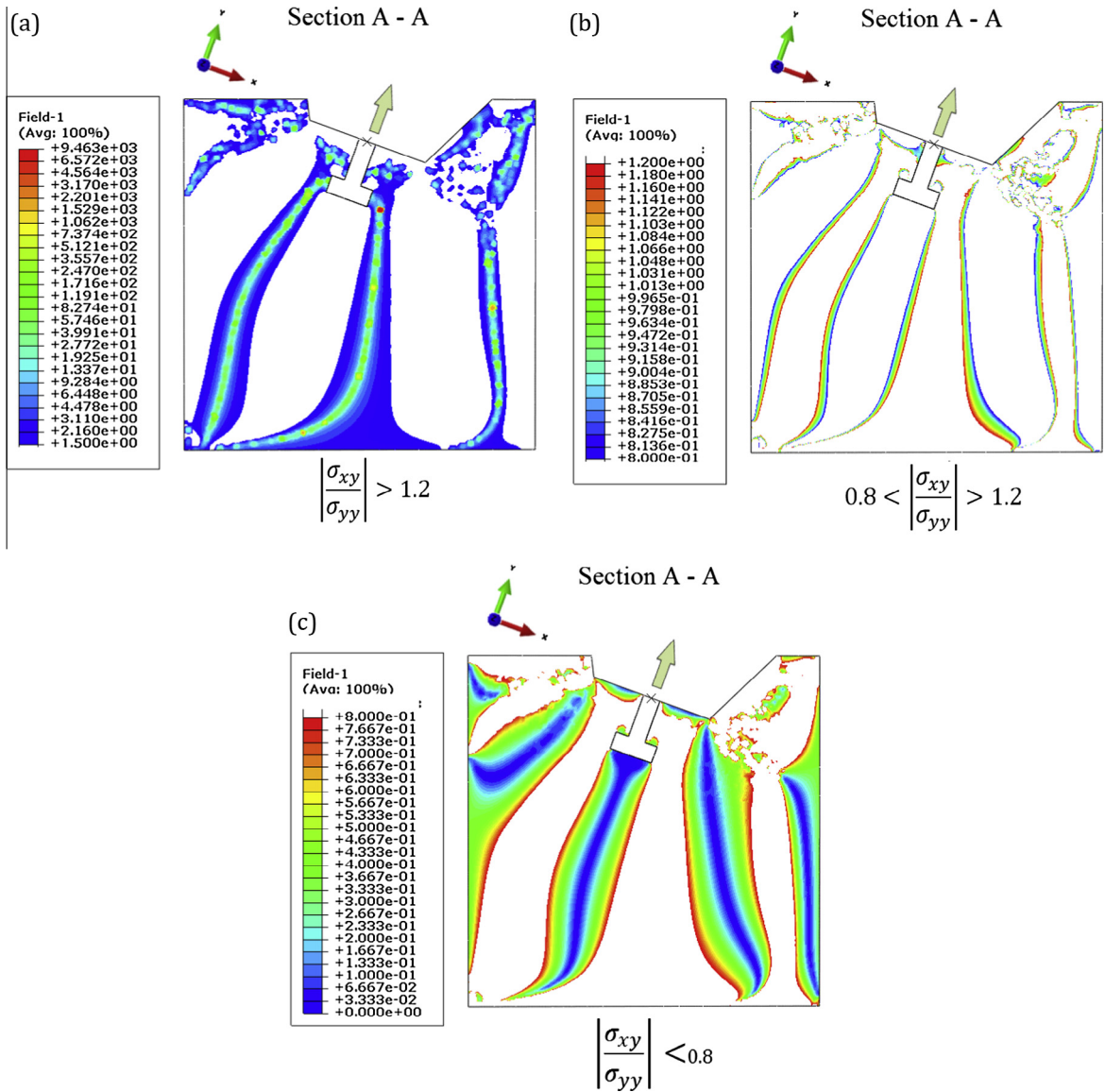
(a) Section A - A

Field-1
(Avg: 100%)

$$\left|\frac{\sigma_{xy}}{\sigma_{yy}}\right| > 1.2$$

(b) Section A - A

Field-1
(Avg: 100%)

$$0.8 < \left|\frac{\sigma_{xy}}{\sigma_{yy}}\right| > 1.2$$

(c) Section A - A

Field-1
(Avg: 100%)

$$\left|\frac{\sigma_{xy}}{\sigma_{yy}}\right| < 0.8$$

**Fig. 14.** Areas of influence of shear stresses (a), combination of shear with normal stresses (b) and normal stresses.



normal stresses

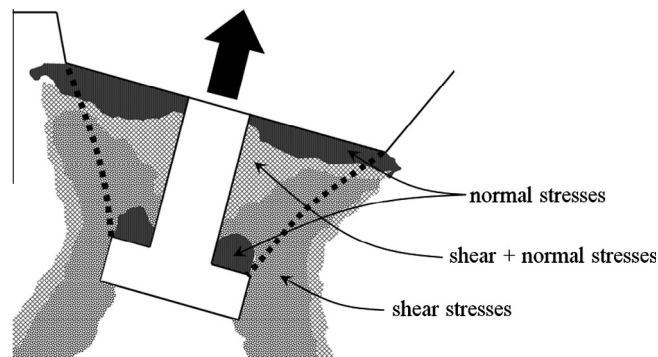shear + normal stresses

shear stresses

**Fig. 15.** Stress mechanism acting on the areas around the steel disk.

increasing the computation power. Additionally, the macroscopic fracture is the result of interaction of several parameters; interphasial strength between the different components (paste-sand, paste-aggregates), strength of paste and aggregate, as well as local stress concentration factors in the microstructure which altogether induce more uncertainty than clarifying the results. The main aim of the present study was focused on quantifying the differences in AE emitted from a nominally uniform compressive stress field, and the pull-out field which certainly includes strong shear components as verified by the analysis of the initial stress field. Though different stress fields may be expected to emit AE signals of different characteristics, before these are quantified in laboratory-controlled studies, the trends cannot be possibly exploited in situ. In this paper this quantification is attempted as a first step towards acoustic structural health monitoring. Investigating the AE signatures of different fracture modes in concrete will contribute in interpreting the trends in real time monitoring applications. Therefore, the condition severity will be possibly evaluated based on shift of simple AE parameters as the ones described in the manuscript, indicating the shift between the different dominant fracture mechanisms.

From the experimental part of the study it is clearly concluded that the normal stresses of the compression test result in higher frequencies and lower RA values of AE signals than the shearing of LOK, as measured by two types of sensors. Specifically, compressive stresses result in double value of emitted frequencies than shear in average (approximately 200 kHz over 100 kHz). RA values exhibit similar differences between the two tests, with the pull-out emitting double values. Still, the specific values of AE parameters assigned to the different modes may not necessarily hold for other specimen geometries or structures. Peak frequencies recorded by the broadband sensors in Fig. 5a would more likely be downshifted for larger specimens and longer propagation distances, with compressive signals maintaining their relatively higher frequency than shear in any case. The reason is connected to the conditions of wave propagation through concrete. It is well known that propagation of elastic waves through heterogeneous media is both attenuative and dispersive [37–39]. This certainly changes the parameters of the waveform from their emission at the tip of the crack until acquisition at the sensor. Distortion and attenuation is active even in small scale influencing the AE signals. This is a matter of great significance when qualitative waveform parameters of the signals are of interest and is treated separately by the authors both by experiments and simulations [40,41]. In this case due to the finite size of the specimens as well as the same positioning of the sensors around all the edges of the cubes for both types of loading, it is assumed that the influence does not crucially mask the observed trends.

It is also worth to mention that using broadband sensors, differences in waveform parameters as well as frequency are readily available between the LOK and compressive test. As has been shown in previous studies broadband sensors are quite suitable for detecting various sources. However, even with resonant sensors, the discrepancies between loading patterns could be distinguished, something important for in-situ application where resonant sensors are preferred due to their higher sensitivity.

## 6. Conclusions

The acoustic emission behavior during different fracture tests on concrete is examined herein. Two tests are used as means to apply different stress conditions on concrete cubes. The basic modes targeted are compression in the standard compressive test and shear during the insert pullout in the form of the LOK test. As FEM analysis indicates, the latter results in a complex state of stress including strong shearing components that overpass normal ones at the area of fracture. The resulting trends show distinct behaviors allowing discrimination of the AE signal populations from the two fracture modes. Fracture due to strong shearing stress components emits waves with longer duration and lower frequency than compression. The passive characterization of the cracking mode can prove very beneficial for structural health monitoring operations as it supplies information that cannot be yielded by any other technique. Discrimination of the modes is accomplished by a few AE parameters which is very encouraging for in-situ application. Apart from this, the analysis can assist material characterization studies in laboratory as it reveals the sensitivities of the material at different stress states.

## References

[1] Shen Z, Yang X, Zhang Z, Cui L, Li T. Microstructure and failure mechanisms of refill friction stir spot welded 7075-T6 aluminum alloy joints. Mater Des 2013;44:476–86.
[2] Shanyavskiy A, Banov M. The twisting mechanism of subsurface fatigue cracking in Ti–6Al–2Sn–4Zr–2Mo–0.1Si alloy. Engng Fract Mech 2010;77:1896–906.

[3] Han Z, Luo H, Cao J, Wang H. Acoustic emission during fatigue crack propagation in a micro-alloyed steel and welds. Mater Sci Engng A 2011;528:7751–6.
[4] Zárate B, Caicedo J, Yu J, Ziehl P. Probabilistic prognosis of fatigue crack growth using acoustic emission data. J Engng Mech 2012;138(9):1101–11.
[5] Iwamoto M, Ni Q-Q, Fujiwara T, Kurashiki K. Intralaminar fracture mechanism in unidirectional CFRP composites Part I: intralaminar toughness and AE characteristics. Engng Fract Mech 1999;64:721–45.
[6] Maillet E, Godin N, R'Mili M, Reynaud P, Fantozzi G, Lamon J. Damage monitoring and identification in SiC/SiC minicomposites using combined acousto-ultrasonics and acoustic emission. Composites: Part A 2014;57:8–15.
[7] Kao C-S, Carvalho FCS, Labuz JF. Micromechanisms of fracture from acoustic emission. Int J Rock Mech Min Sci 2011;48(4):666–73.
[8] Aggelis DG. Classification of cracking mode in concrete by acoustic emission parameters. Mech Res Commun 2011;38:153–7.
[9] Farhidzadeh A, Salamone S, Luna B, Whittaker A. Acoustic emission monitoring of a reinforced concrete shear wall by *b*-value based outlier analysis. Struct Health Monit: Int J 2013;12(1):3–13.
[10] Neville AM. Properties of concrete. Essex, England: Pearson Education Limited; 2011.
[11] Skramtajev BG. Determining concrete strength for control of concrete in structures. J Am Concr Inst 1938;34:285–303.
[12] Carino NJ. Pullout test. In: Malhotra VM, Carino NJ, editors. Handbook on nondestructive testing of concrete. Boca Raton (FL): CRC Press; 1991. p. 39–82 [Chapter 3].
[13] Bungey JH, Millard SG. Partially destructive strength tests, chapter 4 in "Testing of Concrete in Structures". Glasgow: Chapman & Hall; 1996.
[14] Krenchel H, Shah SP. Fracture analysis of the pullout test. Mater Struct 1985;18(108):439–46.
[15] Hellier AK, Sansalone M, Carino NJ, Stone WC, Ingraffea AR. Finite-element analysis of the pullout test using a nonlinear discrete cracking approach. J Cem Concr Aggregates 1987;9(1):20–9.
[16] Grosse CU, Finck F. Quantitative evaluation of fracture processes in concrete using signal-based acoustic emission techniques. Cement Concr Compos 2006;28:330–6.
[17] Ohtsu M, Shigeishi M, Iwase H. Proceedings of the Japan Society of Civil Engineers 408/V-11; 1989, p. 177–86.
[18] Watanabe T, Nishibata S, Hashimoto C, Ohtsu M. Compressive failure in concrete of recycled aggregate by acoustic emission. Constr Build Mater 2007;21:470–6.
[19] Iturrioz I, Lacidogna G, Carpinteri A. Experimental analysis and truss-like discrete element model simulation of concrete specimens under uniaxial compression. Engng Fract Mech 2013;110:81–98.
[20] Cifuentes H, Karihaloo BL. Determination of size-independent specific fracture energy of normal- and high-strength self-compacting concrete from wedge splitting tests. Constr Build Mater 2013;48:548–53.
[21] Rossi P, Tailhan J-L, Le Maou F, Gaillet L, Martin E. Basic creep behavior of concretes investigation of the physical mechanisms by using acoustic emission. Cem Concr Res 2012;42:61–73.
[22] Aggelis DG, Soulioti DV, Gatselou EA, Barkoula N-M, Matikas TE. Monitoring of the mechanical behavior of concrete with chemically treated steel fibers by acoustic emission. Constr Build Mater 2013;48:1255–60.
[23] Carpinteri A, Lacidogna G, Accornero F, Mpalaskas AC, Matikas TE, Aggelis DG. Influence of damage in the acoustic emission parameters. Cement Concr Compos 2013;44:9–16.
[24] Treiber M, Kim J-Y, Qu J, Jacobs LJ. Effects of sand aggregate on ultrasonic attenuation in cement-based materials. Mater Struct 2010;43:1–11.
[25] ASTM C900 Standard Test Method for Pullout Strength of Hardened Concrete.
[26] EN 12504-3 Testing concrete in structures – Part 3: determination of pull-out force.
[27] Claus Germann Petersen, LOK-TEST and CAPO-TEST pullout testing, twenty years experience, Non-Destructive Testing in Civil Engineering Conference in Liverpool, U.K., April 8–11th, 1997, The British Institute of Non-Destructive Testing <http://www.germann.org/TestSystems/LOK-TEST/lok_and_capo_test_correlation.pdf, accessed 1/2014>.
[28] Ohno K, Ohtsu M. Crack classification in concrete based on acoustic emission. Constr Build Mater 2010;24:2339–46.
[29] Shahidan S, Pulin R, Muhamad Bunnori N, Holford KM. Damage classification in reinforced concrete beam by acoustic emission signal analysis. Constr Build Mater 2013;45:78–86.
[30] Shah SG, Chandra Kishen JM. Fracture behavior of concrete–concrete interface using acoustic emission technique. Engng Fract Mech 2010;77:908–24.
[31] Schechinger B, Vogel T. Acoustic emission for monitoring a reinforced concrete beam subject to four-point-bending. Constr Build Mater 2007;21(3):483–90.
[32] Swaddiwudhipong S, Seow PEC. Modelling of steel fiber-reinforced concrete under multi-axial loads. Cem Concr Res 2006;36:1354–61.
[33] Ochoa OO, Reddy JN. Finite element analysis of composite laminates. Kluwer Academic Publishers; 1992.
[34] Invernizzi S, Lacidogna G, Carpinteri A. Particle-based numerical modeling of AE statistics in disordered materials. Meccanica 2013;48(1):211–20.
[35] Carpinteri A, Invernizzi S, Lacidogna G. Historical brick-masonry subjected to double flat-jack test: acoustic emissions and scale effects on cracking density. Constr Build Mater 2009;23:2813–20.
[36] Iturrioz I, Lacidogna G, Carpinteri A. Acoustic emission detection in concrete specimens: experimental analysis and lattice model simulations. Int J Damage Mech 2014;23:327–58.
[37] Vavva MG, Protopappas VC, Gergidis LN, Charalambopoulos A, Fotiadis DI, Polyzos D. Velocity dispersion of guided waves propagating in a free gradient elastic plate: application to cortical bone. J Acoust Soc Am 2009;125(5):3414–27.
[38] Chaix JF, Garnier V, Corneloup G. Ultrasonic wave propagation in heterogeneous solid media: theoretical analysis and experimental validation. Ultrasonics 2006;44:200–10.
[39] Punurai W, Jarzynski J, Qu J, Kurtis KE, Jacobs LJ. Characterization of entrained air voids in cement paste with scattered ultrasound. NDT&E Int 2006;39:514–24.
[40] Aggelis DG, Shiotani T, Papacharalampopoulos A, Polyzos D. The influence of propagation path on acoustic emission monitoring of concrete. Struct Health Monit 2012;11(3):359–66.
[41] Aggelis DG, Mpalaskas AC, Ntalakas D, Matikas TE. Effect of wave distortion on acoustic emission characterization of cementitious materials. Constr Build Mater 2012;35:183–90.